

Cite this: *Nanoscale Adv.*, 2024, 6, 5388

# HF-free microwave-assisted synthesis of MXene as an electrocatalyst for hydrogen evolution in alkaline media†

Kajal Mahabari, <sup>a</sup> Ranjit D. Mohili, <sup>a</sup> Monika Patel, <sup>a</sup> Arvind H. Jadhav, <sup>b</sup> Kwangyeol Lee <sup>\*c</sup> and Nitin K. Chaudhari <sup>\*a</sup>

MXenes, characterized by their robustness, flexibility, and large surface-to-volume ratio facilitating efficient energy transfer with fast response times, have emerged as promising electrocatalysts for hydrogen generation through electrochemical water-splitting. However, the conventional synthetic route to MXenes typically involves the use of hydrofluoric acid (HF) to obtain MXenes with terminal F-functional groups. Unfortunately, these fluorine groups can negatively impact the electrocatalytic performance of MXenes. Moreover, HF is highly toxic, necessitating the development of more environmentally friendly synthetic methods. In response to these challenges, we have developed a novel HF-free microwave-assisted synthesis approach for MXenes. This method harnesses the benefits of uniform heating, homogeneous nucleation, and rapid crystal development, resulting in MXene crystallites with limited size. Importantly, our microwave-assisted approach utilizes a fluoride-free, less hazardous etchant as compared to HF for the synthesis and functionalization of MXene. The as-obtained MXene exhibits significantly improved performance towards the electrochemical hydrogen evolution reaction in alkaline media. Specifically, it demonstrates an overpotential of 140 mV at a current density of 10 mA cm<sup>-2</sup> and a Tafel slope of 84 mV dec<sup>-1</sup>. These results highlight the potential of our HF-free microwave-assisted synthesis approach for producing high-quality MXenes with enhanced electrocatalytic activity for hydrogen generation.

Received 25th March 2024  
Accepted 16th August 2024

DOI: 10.1039/d4na00250d

rsc.li/nanoscale-advances

## 1. Introduction

Conventional energy sources have been crucial in meeting the world's energy demands, but their negative impact on the environment and human health necessitates a shift towards alternative, sustainable options such as solar, wind, biomass, and water energy.<sup>1</sup> Electrochemical water splitting emerges as a promising technique for producing high-purity hydrogen without carbon dioxide emissions, offering a vital solution to contemporary environmental challenges.<sup>2,3</sup> However, the most efficient catalysts for the hydrogen evolution reaction (HER), primarily noble metal-based electrocatalysts such as platinum (Pt) and ruthenium (Ru), are hindered by their high cost and scarcity.<sup>4-9</sup> Indeed, researchers are increasingly focusing on the development of low-cost catalysts with high electro-catalytic

activity to address the growing demand for sustainable energy solutions and to optimize the catalytic performance.<sup>10-13</sup> Among the various materials being explored, two-dimensional (2D) materials have garnered significant interest due to their unique physicochemical properties, atomic-scale thickness, and ease of structural modification.<sup>14-18</sup> The atomic-scale thickness of 2D materials offers several advantages, including a high surface-to-volume ratio, which exposes a larger number of active sites for catalytic reactions.<sup>19-21</sup> Additionally, their tuneable electronic and chemical properties make them highly versatile for various applications. Moreover, the ease of structural modification allows researchers to tailor the properties of 2D materials to suit specific catalytic requirements, further enhancing their performance.<sup>22-24</sup> Overall, 2D materials hold immense potential for catalysis due to their unique characteristics, ease of reaction condition optimization, and exciting electrical properties making them promising candidates for the development of low-cost and efficient catalysts for a wide range of electrochemical processes, including the hydrogen evolution reaction and oxygen reduction reaction, among others.<sup>13,25,26</sup>

In recent years, MXenes, among various 2D materials, have garnered significant attention as catalysts for enhancing electrocatalytic hydrogen production. MXene's excellent conductivity, hydrophilic surface, high surface area, tuneable terminal

<sup>a</sup>Advanced Hybrid Nanomaterial Laboratory, Department of Chemistry, School of Energy Technology, Pandit Deendayal Energy University, Gandhinagar, 382426, Gujarat, India. E-mail: nitin.chaudhari@sot.pdpu.ac.in

<sup>b</sup>Centre for Nano and Material Science (CNMS), Jain University, Jain Global Campus, Bangalore 562112, Karnataka, India

<sup>c</sup>Department of Chemistry, Research Institute for Natural Sciences, Korea University, Seoul 02841, Republic of Korea. E-mail: kylee1@korea.ac.kr

† Electronic supplementary information (ESI) available. See DOI: <https://doi.org/10.1039/d4na00250d>



groups, and numerous reaction sites make it an attractive candidate for the HER. Furthermore, the prolonged lifetime of charge carriers and simple morphological configuration profoundly enhance the catalytic activity.<sup>27,28</sup> The interest in MXenes, particularly Ti-based MXenes, has grown rapidly since the discovery of  $\text{Ti}_3\text{C}_2\text{T}_x$  in 2011.<sup>29</sup> This is mainly attributed to their ease of synthesis and exceptional properties. However, research on MXenes is not limited to Ti systems, and exploration for MXenes beyond titanium is currently underway.<sup>24,25,30</sup> Typically, MXene synthesis involves selectively etching the “A” element from the MAX phase,<sup>31,32</sup> where M is an early transition metal, A is a group IIIA or IVA element, X is C and/or N, and  $n = 1, 2, \text{ or } 3$ .<sup>33</sup> Traditional methods of MXene synthesis, such as using hydrofluoric acid (HF) or molten salts, pose challenges due to safety concerns and high energy consumption.<sup>34–36</sup> Efforts are being made to develop alternative synthesis routes for MXenes that address these challenges and offer safer and more energy-efficient processes. These advancements are crucial for furthering the utilization of MXenes in various applications, including electrocatalytic hydrogen production and beyond.

In this work, we introduce a novel microwave-assisted method for synthesizing MXene, bypassing the need for hazardous HF etchants.  $\text{Ti}_3\text{C}_2\text{T}_x$ , as MXene, has outstanding stability and electrochemical performance. However, its enormous potential has never been completely realised due to restrictions in the self-weight stacking of the layered structure, resulting in inadequate ion-accessible surface area for the electrolyte. MXene production and exfoliation using traditional techniques typically produce thicker MXene sheets with lower lateral dimensions. However, in this work all of the aforementioned constraints can be addressed by employing the microwave-assisted approach. This study presents a novel approach for obtaining a larger lateral size few-layer MXene in a much shorter period (just 30 minutes) than typical etching procedures, by employing microwave radiation to quickly evaporate interlayer water.<sup>37</sup> The microwave-assisted technique offers several advantages, including rapid crystallization, cost-effectiveness, ease of operation, phase selectivity, controlled material size, rapid heating, high reaction rates, and morphology control.<sup>38,39</sup> Our unique microwave-assisted fluoride-free NaOH-based chemical reduction technique enables quick reactions and intercalates the ions into the sheets, resulting in the formation of crumpled sheet-like morphology MXene. The key improvements in the MXene synthesized with microwave assistance include elimination of the need for a hydrothermal reactor, allowing for the reaction to take place in an open vessel. Lastly, utilization of an alkali (NaOH) as an innocuous etchant compared to hazardous HF based etching and intercalated agents ensures safety and quite environmental friendliness. The resultant microwave-assisted MXene, referred to as MMXene (where “M” denotes microwave), has been characterized using various physical analysis techniques, confirming the successful synthesis of MXene with crumpled sheet-like morphology. When evaluated for electrochemical water splitting, 2D MMXene nanosheets exhibited exceptional performance in hydrogen evolution reaction (HER)

activity, demonstrating a low overpotential of 140 mV at a current density of  $10 \text{ mA cm}^{-2}$  and a Tafel slope of  $84 \text{ mV dec}^{-1}$ . To our knowledge, this is the first report of implementing a non-HF-based microwave-assisted synthesis of MXene nanosheets for electrocatalytic hydrogen evolution. These findings highlight the potential of our approach to produce high-quality MXene catalysts for various applications in sustainable energy conversion.

## 2. Experimental section

### 2.1 Materials and methods

MAX phase titanium aluminium carbide ( $\text{Ti}_3\text{AlC}_2$ ) was purchased from Nanoshell Co. Ltd, India, while lithium fluoride (LiF), 98.5%, was obtained from Alfa Aesar. Nafion solution was purchased from the fuel cell store, and nickel foam was sourced from IPGI Chennai, India. All other chemicals of analytical grade were acquired from Finar Chemicals, India, and were used without additional purification. Deionized water was utilized in all experiments to ensure consistency and accuracy of results.

**2.1.1 Microwave-assisted synthesis of MXene.** MXene ( $\text{Ti}_3\text{C}_2$ ) was synthesized *via* a microwave-assisted reduction method as illustrated in Fig. 1. In this process, MAX phase titanium aluminium carbide ( $\text{Ti}_3\text{AlC}_2$ ) was utilized as the precursor for the formation of MXene  $\text{Ti}_3\text{C}_2$ , while sodium hydroxide (NaOH) served as both an etchant and a reducing agent. In brief, 100 ml of 2 M NaOH solution and 1 g of  $\text{Ti}_3\text{AlC}_2$  precursor were mixed and placed in a microwave at 210 W for 30 minutes. Following the microwave treatment, the resulting black powder was collected and subjected to repeated washing with ethanol and distilled water. Finally, the washed products were dried at  $60 \text{ }^\circ\text{C}$  in an oven overnight, resulting in the formation of blackish powder of MMXene.

**2.1.2 LiF synthesis approach for MXene.** Additionally,  $\text{Ti}_3\text{C}_2\text{T}_x$  was synthesized *via* a modified etching route following earlier reports.<sup>40</sup> In this method, 1 g of LiF was dissolved in 20 ml of HCl in a 100 ml polypropylene plastic vial to create the etchant solution for the LiF technique. Subsequently, 1 g of  $\text{Ti}_3\text{AlC}_2$  precursor was slowly added to the mixture, and the reaction was allowed to proceed for 24 hours at  $35 \text{ }^\circ\text{C}$ . The acidic product obtained was thoroughly washed with deionized water ( $\text{DI H}_2\text{O}$ ) *via* centrifugation at 3500 rpm until the pH of the solution reached or exceeded 6. Following centrifugation for 1 hour, a dark black solution containing large  $\text{Ti}_3\text{C}_2\text{T}_x$  flakes was collected.<sup>41</sup>

### 2.2 Materials characterization

The scanning electron microscopy (FE-SEM) analysis was conducted to examine the morphology of the materials. The FE-SEM utilized was model JSM-IT200 by JEOL Ltd, operated at a voltage of 20 kV. For examining the crystalline structures of the materials, X-ray diffraction (XRD) analysis was performed using a D2 Phaser model with a diffractometer using Cu target ( $\lambda = 1.54 \text{ \AA}$ ) radiation, with a scanning range from  $3$  to  $160^\circ$  and



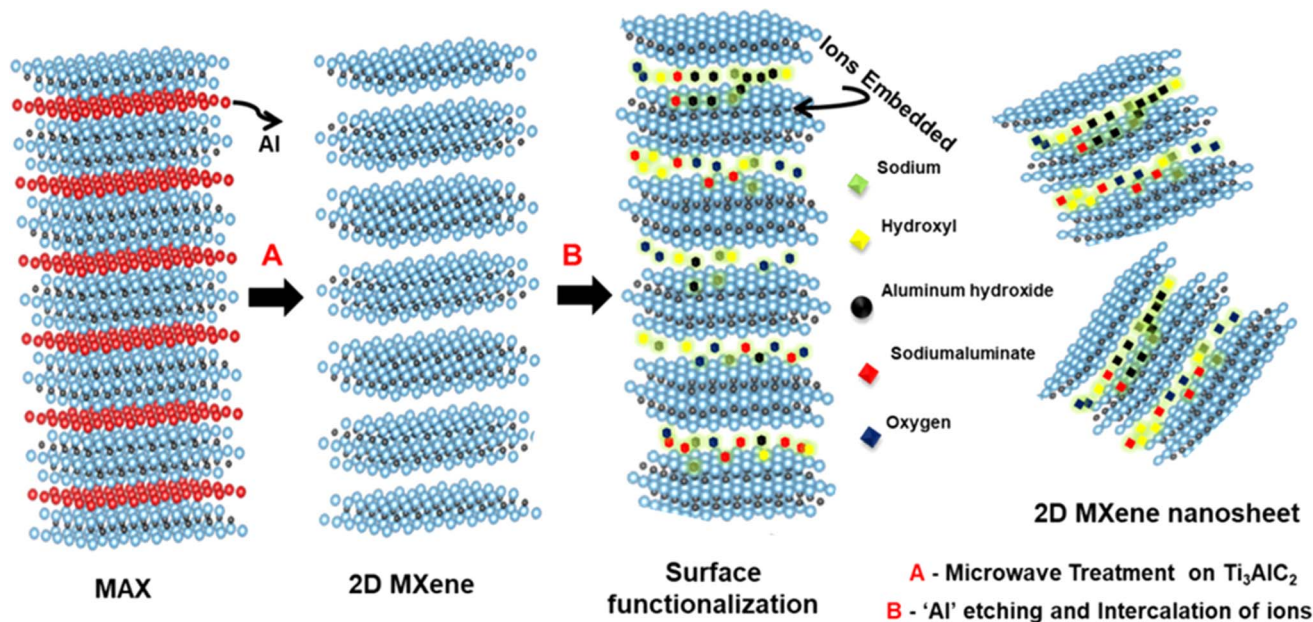


Fig. 1 Schematic representation of microwave assisted synthesis of MXene.

a step scan of  $0.05^\circ$ . Elemental analysis was carried out using FTIR PerkinElmer analytical instruments.

### 2.3 Electrochemical measurements

First, nickel foam (NF) (length  $\times$  breadth =  $1 \times 1$  cm, IPGI instruments, Chennai, India) was cleaned by sonication using hydrochloric acid, ethanol and water for 15 min each and dried in an oven. 10 mg of MMXene was synthesised by using the microwave-assisted approach, and 10  $\mu$ l of Nafion solution and 400  $\mu$ l of water were mixed and sonicated to obtain a uniform slurry. We employed Ni foam as a substrate; however, distinct from other substrates, Ni foam is porous, has a high catalytically active surface area, and is resistant to corrosion in alkaline solution.<sup>42</sup> This slurry (200  $\mu$ l) was then cast drop by drop on Ni foam ( $\text{Ti}_3\text{C}_2\text{T}_x/\text{NF}$ ), which was then dried on a hot plate to obtain 20 mg mass deposition and finally dried at  $60^\circ\text{C}$  in an oven for 1 h. Hydrogen evolution activity of the catalysts was measured using an electrochemical workstation (Autolab Instrument Inc.) in a conventional three-electrode configuration with 2 M NaOH electrolyte (99.99%) at room temperature. Glassy carbon is used as a counter electrode material in three-electrode setups for electroanalytical chemistry. A silver chloride electrode (Ag/AgCl) was used as the reference electrode and  $\text{Ti}_3\text{C}_2\text{T}_x/\text{NF}$  was used as the working electrode. Before electrochemical measurements, 2 M NaOH was purged with highly pure  $\text{N}_2$  gas (99.99%) to remove any interfering gases such as  $\text{H}_2$ ,  $\text{O}_2$ , etc. All data were presented after the conversion to the reversible hydrogen electrode (RHE) scale using the Nernst equation ( $E = E_0 + E_{\text{Ag/AgCl}} + 0.059 \times \text{pH}$ ,  $E_{\text{Ag/AgCl}} = 0.1976$  V). The electrocatalytic HER performance of the samples was evaluated by linear sweep voltammetry (LSV) and cyclic voltammetry (CV) with a scanning rate of  $500 \text{ mV s}^{-1}$  with potential range  $-1.4$  to  $0$  V and  $-2$  to  $1.5$  V respectively. The

electrochemical impedance spectroscopy (EIS) was conducted (Nyquist plot) in a frequency range of 1000 kHz to 0.01 Hz and at a voltage of 1 V.

## 3. Results and discussion

### 3.1 Physical characterization

The XRD analysis provided valuable insights into the structural changes occurring during the synthesis of MXene from the MAX phase  $\text{Ti}_3\text{AlC}_2$ . The characteristic peaks observed in the XRD patterns confirm the presence of specific crystallographic planes in both MAX and MXene phases as shown in Fig. 2a, where the characteristic peaks at  $9.8^\circ$  and  $38.9^\circ$  correspond to (002) of stacked layers in the MAX phase and (104) of 'Al' atomic arrangement, respectively.<sup>43</sup> The shift in the (002) peak towards a lower angle in the MXene compared to the MAX phase indicates an increase in the interlayer spacing, suggesting successful extraction of aluminium atoms and formation of MXene. The near disappearance of the (104) peak further supports the removal of aluminium from the  $\text{Ti}_3\text{AlC}_2$  MAX phase.<sup>44</sup> The narrow peaks in the XRD pattern indicate the crystalline nature of the MMXene sheets, with well-arranged atoms or ions in highly ordered structures. Overall, the XRD data provide compelling evidence for the successful synthesis of MXene from the  $\text{Ti}_3\text{AlC}_2$  MAX phase.

The FTIR spectrum of MMXene revealed several bands corresponding to different functional groups as shown in Fig. 2b. These include Ti-C, Ti-O, C-Cl, Al-OH, C=C, C=O, O=C=O, C-H, and Na-OH at wavenumbers 525, 682, 850, 1060, 1610, 1820, 2111, 2340, 2668,  $3130 \text{ cm}^{-1}$ , respectively. The presence of these bands indicates the presence of various chemical bonds and functional groups in the MMXene structure. For instance, the Ti-C and Ti-O bands suggest the presence of titanium-



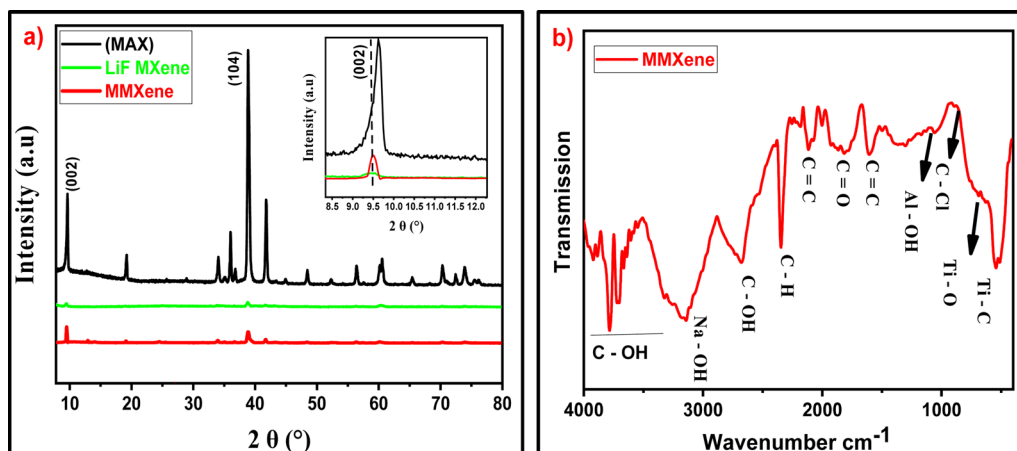


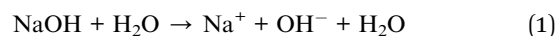
Fig. 2 Physical characterization of MMXene, (a) XRD and (b) FTIR.

carbon and titanium–oxygen bonds, respectively. The C–Cl band indicates the presence of chlorine-containing compounds, while the presence of C=C and C=O bands indicates the presence of carbon–carbon double bonds and carbonyl groups, respectively. The O=C=O band suggests the presence of carbon dioxide due to an open environment reaction. The C–H band indicates the presence of carbon–hydrogen bonds, and the Na–OH band suggests the presence of sodium hydroxide residues. Furthermore, the presence of C–OH bands in the region of 3500 to 3800  $\text{cm}^{-1}$  suggests the involvement of hydroxyl groups resulting from the reaction between the MAX phase and the solvent.<sup>45</sup> The FTIR data also indicate the hydrophilic nature of MMXene due to the presence of oxygen and hydroxyl groups.<sup>46</sup> However, the weak bands from these moieties suggest their low concentration or intensity. The presence of sodium, as indicated by the Na–OH band, further confirms the involvement of NaOH solution in the synthesis process. The EDX analysis provides complementary information regarding the elemental composition of MMXene, corroborating the findings from the FTIR analysis and confirming the high purity of the synthesized MXene.<sup>47</sup>

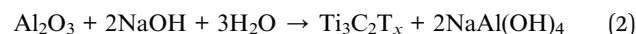
The successful synthesis of  $\text{Ti}_3\text{C}_2$  and the formation of a crumpled lamellar-like sheet structure were observed through Scanning Electron Microscope (SEM) analysis which is helpful for effective hydrogen generation application, as depicted in Fig. 3c. The basal planes of  $\text{Ti}_3\text{C}_2$  exhibited buffing due to microwave irradiation, attributed to the replacement of the Al atom layer by  $\text{T}_x$  (intercalated ions). The SEM image of MMXene clearly demonstrates the engineered crumpled lamellar-like sheet structure with desirable inter-planar spacing achieved through aluminium etching. In MMXene, the presence of excess O and Na signals can be attributed to surface terminations (–Na and/or –O and –OH) as well as intercalated water and sodium ions between  $\text{Ti}_3\text{C}_2$  layers, as revealed by Energy Dispersive Spectroscopy (EDS) analysis shown in Fig. 3d.<sup>48</sup> The residual Al signal may originate from the reaction product  $\text{Al}(\text{OH})_4$ , which might not have been completely washed away. However, the EDS spectrum confirms that the chemical compositions of MMXene primarily consist of Ti, C, O, and Na.<sup>49</sup>

### 3.2 Synthesis mechanism of MXene

In this study, a microwave-assisted route was employed for the synthesis of MXene, utilizing a HF-free etchant, sodium hydroxide, and MAX phase  $\text{Ti}_3\text{AlC}_2$  as the MXene precursor. This approach leverages the alignment of dipoles within the material induced by external fields generated by microwave electromagnetic radiation.<sup>50</sup> When dielectric materials absorb microwaves, they undergo molecular motion, causing ionic species to migrate and dipolar species to rotate. Unlike heat convection and conduction, microwave heating promotes the fragmentation of large precursor molecules and accelerates the breakage of chemical bonds.<sup>51</sup> Importantly, microwave irradiation facilitates interactions among a higher number of ions, thereby enhancing catalytic processes in a shorter duration. This is considered a key advantage of microwave etching for obtaining desirable MXene materials. When MAX phase  $\text{Ti}_3\text{AlC}_2$  is introduced into a NaOH solution, it disperses in water. Irradiation induces friction with water, generating heat and leading to the dissociation of ions such as sodium ( $\text{Na}^+$ ) and hydroxyl ( $\text{OH}^-$ ), as depicted in eqn (1).



Subsequently,  $\text{Ti}_3\text{AlC}_2$  undergoes dissociation and friction, leading to the breakage of Ti and Al bonds and the formation of  $\text{Al}_2\text{O}_3$ . This  $\text{Al}_2\text{O}_3$  then etches out from the parent MAX phase as sodium aluminate hydrate ions, as illustrated in eqn (2). The resulting sodium aluminate hydrate ( $\text{NaAl}(\text{OH})_4$ ) can be readily separated due to its dissociation in water, resulting in the formation of  $\text{Ti}_3\text{C}_2\text{T}_x$ .



Accordingly, the remaining  $\text{NaAl}(\text{OH})_4$  further dissociates into  $\text{Na}^+$  and  $\text{Al}(\text{OH})_4^-$ . As Al is etched out, these ions subsequently get intercalated into the MXene as hydroxide and sodium, which originate from the solution, along with oxygen from the air. As a result, we have successfully synthesized



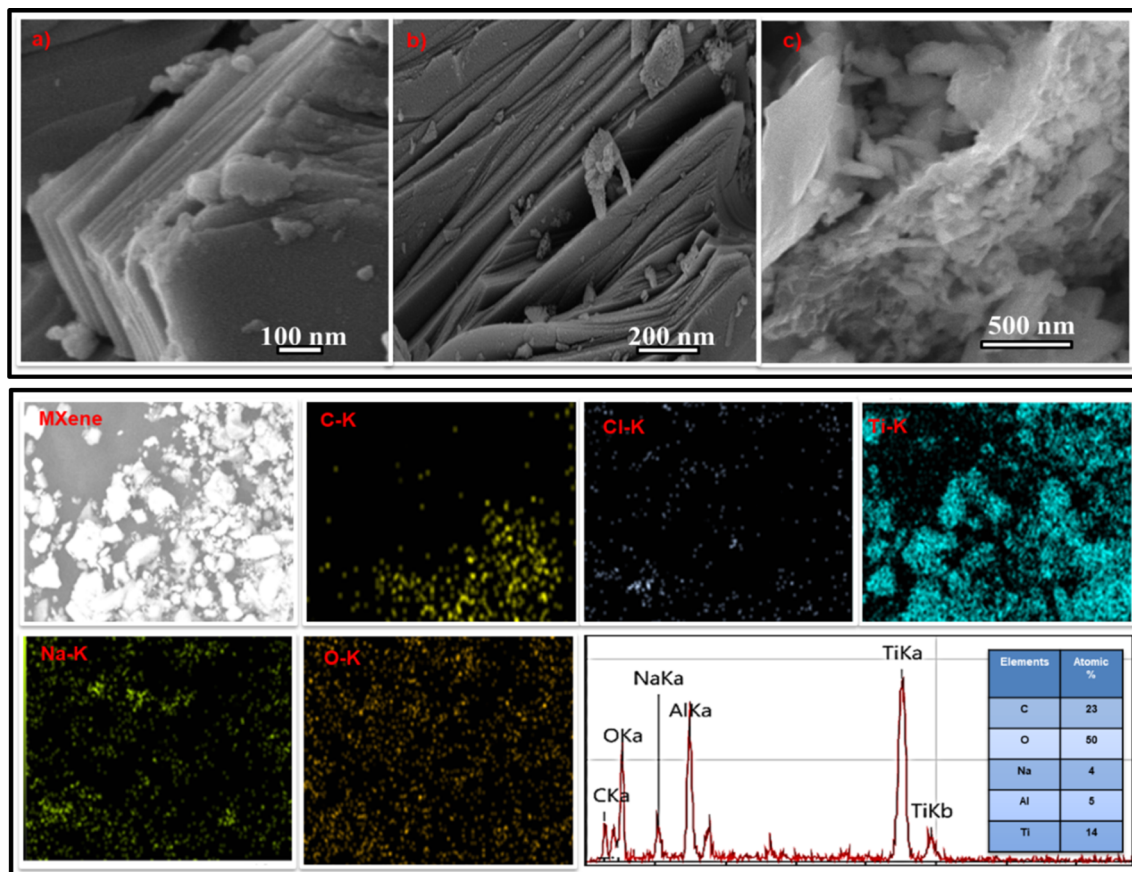
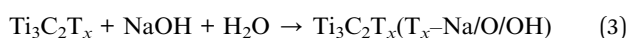


Fig. 3 SEM image of (a) MAX phase, (b) LiF MXene and (c) MMXene. (d) EDS and elemental mapping of MMXene.

MXene via a microwave-assisted route using HF-free etchant NaOH and  $\text{Ti}_3\text{AlC}_2$  (Table 1).



### 3.3 Electrochemical activity

To evaluate the electrocatalytic activity towards the hydrogen evolution reaction (HER), MMXene was drop-cast onto nickel foam (NF) using Nafion as a binder (mass loading:  $20 \text{ mg cm}^{-2}$ ). The MMXene@NF electrode materials were then analysed in a three-electrode electrochemical cell in 2 M NaOH through cyclic voltammetry (CV), linear sweep voltammetry (LSV), Tafel plot, and electrochemical impedance spectroscopy measurements. In the LSV in Fig. 4a, it is depicted that the hydrogen

evolution overpotential of MXene synthesized using LiF and MMXene as working electrodes at  $10 \text{ mA cm}^{-2}$  is 370 and 140 mV, respectively. The lower overpotential of MMXene synthesized by the microwave-assisted approach could be attributed to the insertion of a number of sodium, oxygen, hydroxyl ions, and hydroxo aluminate ions, which participate in the catalytic reaction to accelerate the process. Furthermore, MMXene showed the highest current density in a potential window of  $-1.0$  to  $0 \text{ V}$ . MMXene basal planes have numerous functionalized active sites, and LiF-assisted etching techniques promote fluorine functionalization on the basal planes, reducing the materials HER catalytic activity. Although hydrogen adsorption (GH) energy close to zero is preferred for efficient HER activity, density functional theory (DFT) studies of fluorine-functionalized MXene reveal that the GH value

Table 1 Comparison of microwave-assisted synthesised MXene to prior methods for electrochemical hydrogen generation in alkaline electrolytes

MXene	Synthesis approach	Electrolyte	Overpotential (mV)@ $10 \text{ mA cm}^{-2}$	Tafel slop ( $\text{mV dec}^{-1}$ )	References
$\text{Ti}_3\text{C}_2\text{T}_x$	Microwave	NaOH	140	84	This work
	<i>In situ</i> HF	KOH	218	156	52
	HF	NaOH	1000	—	53
	<i>In situ</i> HF	KOH	344	216	54
	<i>In situ</i> HF	KOH	532	101	55
	<i>In situ</i> HF	KOH	541	468	56



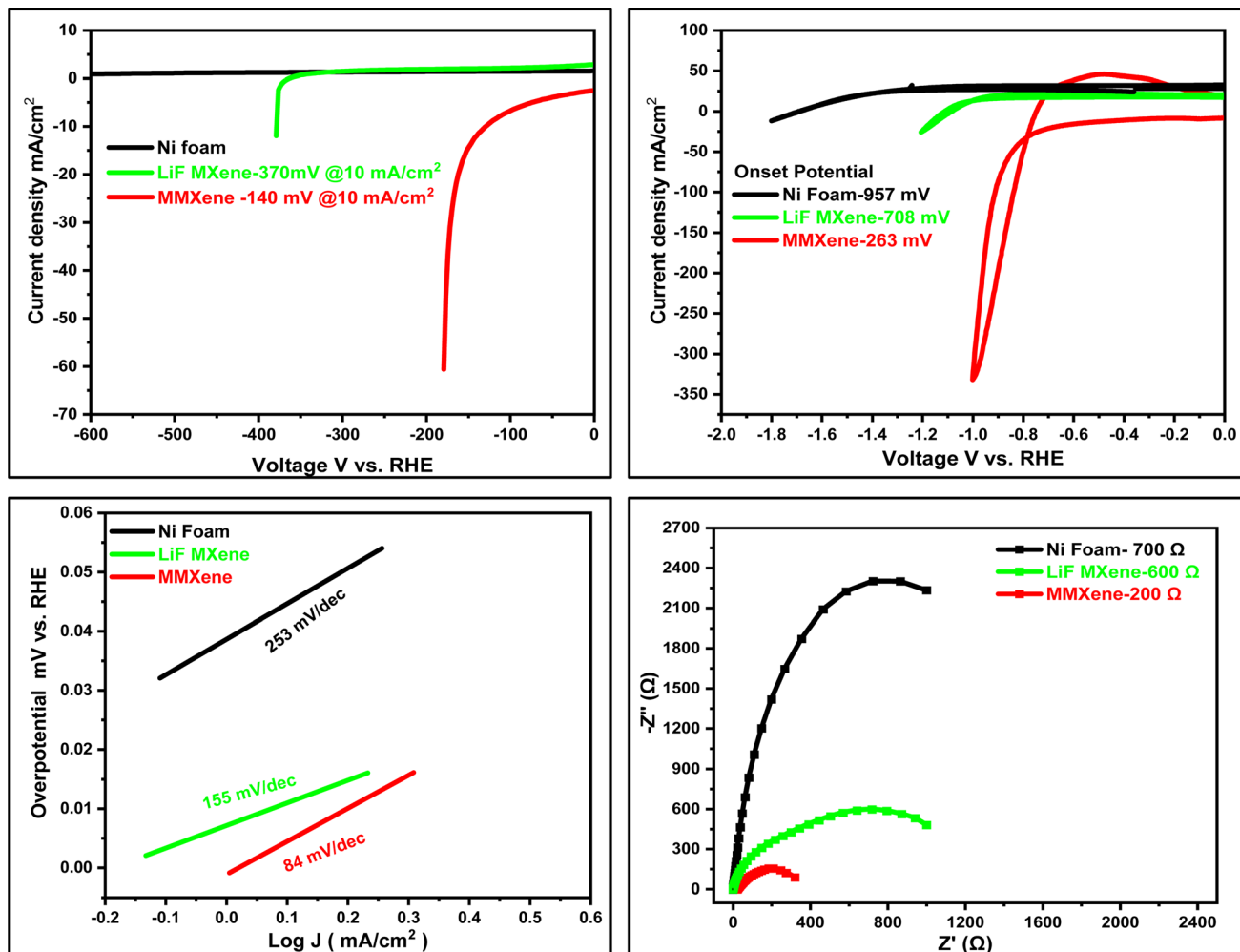


Fig. 4 Electrochemical characterization of MMXene, (a) LSV, (b) CV, (c) Tafel plot and (d) impedance spectra.

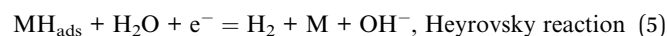
increases with fluorine surface coverage.<sup>57</sup> Fluorine-free methods mitigate the adverse effects of -F terminations on MXene conductivity, improving electronic properties.<sup>58</sup> Furthermore, oxygen and hydroxyl functional groups have been shown to increase HER activity while significantly reducing overpotential.<sup>59</sup> As a result, fluorine-free procedures are strongly recommended for electrochemical hydrogen production.

CV was used to further investigate how the ions alter the kinetics of the hydrogen evolution reaction, which was recorded from -2 to 1.5 V at 100 mV s<sup>-1</sup>. As shown in Fig. 4b, a CV curve at 100 mV s<sup>-1</sup> for the bare Ni foam catalyst, LiF MXene (20 mg cm<sup>-2</sup> mass loading) and MMXene deposited on Ni foam (20 mg cm<sup>-2</sup> mass loading) was recorded. For the MMXene catalyst, the HER onset potential occurs at about 263 mV vs. RHE as indicated by a sudden increase in the cathodic current as shown in Fig. 4b, while for bare Ni foam and LiF MXene it occurs at 957 mV and 708 mV, respectively.<sup>60</sup> The MMXene catalyst displayed better activity for hydrogen evolution with current density 62 mA cm<sup>-2</sup>, which is much higher as compared to that of bare Ni foam and LiF MXene. The better electrocatalytic activity of the MMXene electrode is mainly attributed to the thin

lamellar MMXene nanosheet with desirable distance between the Ti<sub>3</sub>C<sub>2</sub>T<sub>x</sub> layers and efficient electron transfer, resulting in better access of electrolyte to the catalytically active surface.<sup>61</sup> The surface area of the electrocatalyst was assessed using the capacitance approach, which involved analysing cyclic voltammetry (CV) data obtained at different scan rates, ranging from 50 to 200 mV s<sup>-1</sup>. The electrochemical surface area (ECSA) was subsequently calculated based on these measurements. This process entailed determining the double-layer capacitance (C<sub>dl</sub>) values from the CV curves. The double-layer capacitance (C<sub>dl</sub>) values for the samples were determined by graphing (|J<sub>a</sub>| - |J<sub>c</sub>|) against the cyclic voltammetry (CV) scan rate. This involved plotting the absolute difference between the anode current density (J<sub>a</sub>) and the cathode current density (J<sub>c</sub>) against the scan rate. The resulting graph allowed for the calculation of C<sub>dl</sub> values, which are crucial for assessing the electrochemical surface area (ECSA) of the samples.<sup>62</sup> Furthermore, the observed improvements in electrochemical activity can be attributed to the composition of the MMXene, which lacks fluorine groups (F) and primarily consists of hydroxyl groups (-OH), sodium groups (-Na), oxygen groups (-O), and hydroxo aluminate



groups ( $-\text{AlOH}$ ). To better understand the kinetics of the hydrogen evolution reaction (HER) catalysed by MMXene, the rate-determining steps were investigated using Tafel slope analysis, as shown in Fig. 4c. The Tafel slopes obtained for bare Ni foam, LiF MXene, and MMXene are 253, 155, and 84  $\text{mV dec}^{-1}$ , respectively. Considering that Tafel analysis was conducted using the current response at low overpotential, it is likely that the Volmer step serves as the rate-determining step. This change in the reaction mechanism on MMXene suggests that intercalated ions play a crucial role in accessing the surface for hydrogen adsorption and desorption. It is widely accepted that the HER under alkaline conditions proceeds *via* a three-step mechanism.<sup>63,64</sup>



As illustrated in Fig. 4d, electrochemical impedance spectroscopy (EIS) was employed to investigate the charge carrier recombination/transfer behaviour of MMXene. The MMXene electrocatalyst demonstrated the smallest arc size on the Nyquist curve, indicating high conductivity that facilitates easy electron migration. In contrast, LiF MXene exhibited a larger radius of the arc, suggesting an increase in carrier transfer impedance. In the Nyquist diagram, the impedance value reflects the resistance in the transfer of charges during the hydrogen evolution reaction (HER). A smaller arc radius corresponds to a lower impedance value of the test sample, indicating a greater likelihood of the hydrogen evolution catalytic reaction occurring. The charge transfer resistance is determined by the size of the semicircle and the properties of the electrode surface. The charge transfer resistance values for pure Ni foam, LiF MXene, and MMXene are 700, 600, and 200  $\Omega$ ,

respectively. This suggests that MMXene exhibits significantly lower charge transfer resistance compared to Ni foam and LiF MXene, further highlighting its superior electrochemical performance in facilitating the hydrogen evolution reaction.

To account for the challenge in determining the mass of the etched layer, the electrochemical surface area (ECSA) values were represented per unit of surface area, expressed as real capacitances ( $\text{F cm}^{-2}$ ). This approach allows for a standardized comparison of ECSA values across different samples, irrespective of variations in the mass of the etched layer. As depicted in Fig. 5a, the measured double-layer capacitance (Cdl) for the MMXene electrocatalyst was found to be  $14.2 \text{ mF cm}^{-2}$ . This increased average Cdl value compared to earlier reports suggests that the MMXene offers a larger electro-active surface area, which is beneficial for electrochemical performances.<sup>65</sup> Additionally, Fig. 5b demonstrates the excellent stability of MMXene in alkaline electrolyte. The potential of the catalyst remains stable at 260 mV during continuous electrolysis at  $10 \text{ mA cm}^{-2}$  for a duration of 9 hours. This stability underscores the potential utility of MMXene as an electrocatalyst in various applications. The voltage gradually decreased from 315 to 266 mV to maintain a current density of  $10 \text{ mA cm}^{-2}$  for the first hour and 15 min. There was no significant drop in potential for the remaining 9 hours and 25 min. Over a period of time, the potential remains constant for up to almost 9 hours and 25 min, indicating that the synthesized catalyst is stable in electrochemical hydrogen production with no potential reduction.

To analyse the structural stability of the MMXene/Ni electrode, we conducted XRD and FE-SEM analysis after a long term stability test as shown in Fig. S1.† Fig. S1a† shows the XRD pattern of the MMXene/Ni electrode before and after the electrochemical stability test (after 10 h). There were minor differences observed, such as the characteristic diffraction peak of the MMXene nanostructure (indicated by \*) becoming broadened due to long-term ion intercalation into the layered sites of the MMXene nanostructures. Fig. S1b† confirms that there is no

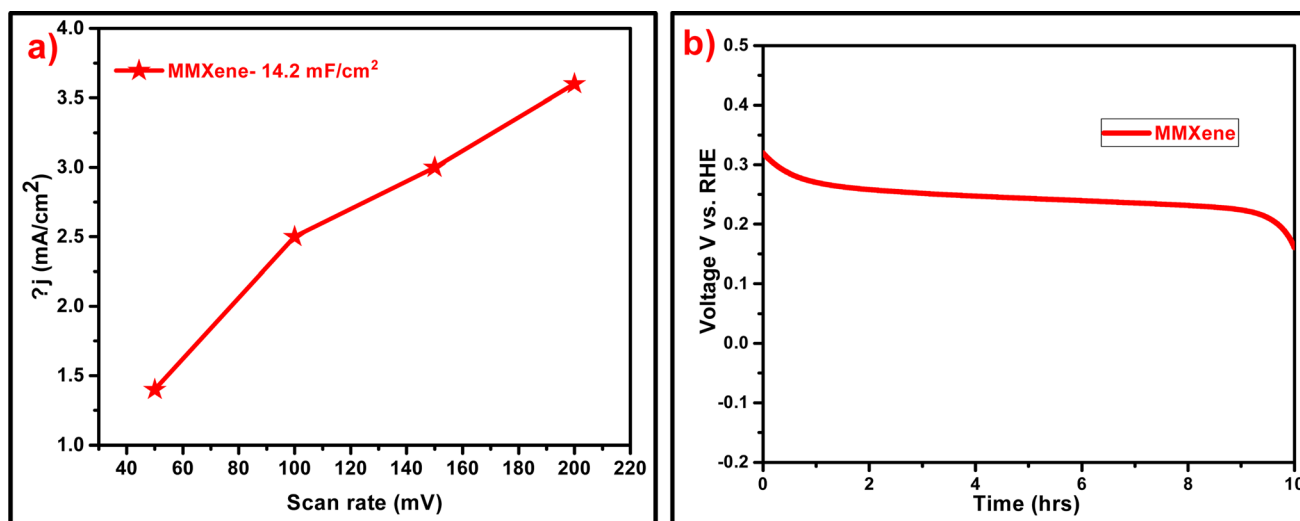


Fig. 5 (a) ECSA plots inferred from CV curves at different scan rates. (b) Chronopotentiometry curve at a constant current density of  $10 \text{ mA cm}^{-2}$  for the MMXene catalyst in 2 M NaOH.



significant change in the morphology of the MMXene/Ni electrode after electrochemical stability tests, which highlights the good adherence of the MMXene on the Ni foam. The ion adsorption on the surface of MXene converts the morphology of the thin crumbled layer to a thick, rough surface. The XRD and FE-SEM results indicate that the MMXene/Ni foam possesses good structural stability in an alkaline electrolyte towards the hydrogen evolution reaction.

## 4. Conclusion

In summary, MXene with 2D structures was prepared using the microwave-assisted etching method, and its electrochemical activities towards hydrogen evolution were investigated. This novel microwave-assisted approach offers increased reaction kinetics, rapid initial heating, and enhanced reaction rates, resulting in clean reaction products. Notably, this approach required less time (30 minutes) for the reaction, with the functionalization of MMXene facilitated by the presence of several functional groups. The as-synthesized MMXene exhibited outstanding catalytic activity in alkali electrolyte, as demonstrated by EDS analysis revealing the presence of various terminations in MMXene, which aids in more efficient electron transfer. In contrast to earlier synthesis approaches for MXene involving HF or *in situ* HF etching, microwave-assisted synthesized MXene overcomes drawbacks such as the use of toxic chemicals, fluorine functionalization, amorphous nature, unstable structure, and inadequate electron transport. Microwave-assisted synthesized MXene has been identified as an efficient electrocatalyst for hydrogen generation through electrochemical water splitting compared to previously reported MXenes. The excellent performance of the  $\text{Ti}_3\text{C}_2\text{T}_x$  (O, OH, AlOH, and Na ions) catalyst in the hydrogen evolution reaction (HER) can be attributed to several key characteristics: high coverage of catalytically active O terminations on the basal planes, ultrathin nanosheet architecture exposing more active sites, and the presence of numerous terminations. Furthermore, F-free MXene from this study exhibits effective electronic conductivity, facilitating excellent charge transfer, which is crucial for efficient hydrogen generation.

## Conflicts of interest

All data underlying the results are available as part of the article itself and no additional data are required.

## Acknowledgements

This study was supported by the Central Power Research Institute (CPRI), Bangalore (RSOP/21-26/GD/6) and Pandit Deendayal Energy University (PDEU) under the start-up grant ORSP/R&D/PDPU/2021/NC00/R0069 as well as NRF-2020K1A3A1A19088726. The authors would like to thank Shivaji University, Kolhapur and the Indian Institute of Technology, Gandhinagar, for allowing the usage of XRD, XPS and FESEM, respectively. Also, we thank YCIS Satara and PDEU, Gandhinagar, for allowing the usage of SEM, EDX and FTIR.

## References

- 1 M. Rafique, *et al.*, A Comprehensive Study on Methods and Materials for Photocatalytic Water Splitting and Hydrogen Production as a Renewable Energy Resource, *J. Inorg. Organomet. Polym. Mater.*, 2020, **30**(10), 3837–3861, DOI: [10.1007/s10904-020-01611-9](https://doi.org/10.1007/s10904-020-01611-9).
- 2 S. Wang, A. Lu and C.-J. Zhong, Hydrogen production from water electrolysis: role of catalysts, *Nano Convergence*, 2021, **8**(1), 4, DOI: [10.1186/s40580-021-00254-x](https://doi.org/10.1186/s40580-021-00254-x).
- 3 X. Li, *et al.*, Water Splitting: From Electrode to Green Energy System, *Nano-Micro Lett.*, 2020, **12**(1), 131, DOI: [10.1007/s40820-020-00469-3](https://doi.org/10.1007/s40820-020-00469-3).
- 4 C. Li and J.-B. Baek, Recent Advances in Noble Metal (Pt, Ru, and Ir)-Based Electrocatalysts for Efficient Hydrogen Evolution Reaction, *ACS Omega*, 2020, **5**(1), 31–40, DOI: [10.1021/acsomega.9b03550](https://doi.org/10.1021/acsomega.9b03550).
- 5 B. H. Park, *et al.*, Synergistic Ru-Ni-Cu interface for stable hydrogen evolution on 1% Ru-Ni@Cu alloy grown directly on carbon paper electrode, *J. Alloys Compd.*, 2022, **913**, 165315, DOI: [10.1016/j.jallcom.2022.165315](https://doi.org/10.1016/j.jallcom.2022.165315).
- 6 B. Wang, *et al.*, Room-Temperature Laser Planting of High-Loading Single-Atom Catalysts for High-Efficiency Electrocatalytic Hydrogen Evolution, *J. Am. Chem. Soc.*, 2023, **145**(25), 13788–13795, DOI: [10.1021/jacs.3c02364](https://doi.org/10.1021/jacs.3c02364).
- 7 B. Wang, *et al.*, General synthesis of high-entropy alloy and ceramic nanoparticles in nanoseconds, *Nat. Synth.*, 2022, **1**(2), 138–146, DOI: [10.1038/s44160-021-00004-1](https://doi.org/10.1038/s44160-021-00004-1).
- 8 G. Zhong, S. Xu and B. Fang, Single Pt atomic sites anchored on 1T' phase MoS<sub>2</sub> nanosheets towards efficient hydrogen evolution, *Materials Today Catalysis*, 2024, **4**, 100045, DOI: [10.1016/j.mtcata.2024.100045](https://doi.org/10.1016/j.mtcata.2024.100045).
- 9 L. Lu, H. Zheng, Y. Li, Y. Zhou and B. Fang, Ligand-free synthesis of noble metal nanocatalysts for electrocatalysis, *Chem. Eng. J.*, 2023, **451**, 138668, DOI: [10.1016/j.cej.2022.138668](https://doi.org/10.1016/j.cej.2022.138668).
- 10 W. Moschkowitsch, O. Lori and L. Elbaz, Recent Progress and Viability of PGM-Free Catalysts for Hydrogen Evolution Reaction and Hydrogen Oxidation Reaction, *ACS Catal.*, 2022, **12**(2), 1082–1089, DOI: [10.1021/acscatal.1c04948](https://doi.org/10.1021/acscatal.1c04948).
- 11 J. Min, *et al.*, Atomically dispersed platinum electrocatalysts supported on gadolinia-doped ceria nanoparticles for practical high-temperature solid oxide cells, *J. Mater. Chem. A*, 2023, **11**(46), 25298–25307, DOI: [10.1039/D3TA05534E](https://doi.org/10.1039/D3TA05534E).
- 12 N. Han, X. Zhao and V. K. Thakur, Adjusting the interfacial adhesion via surface modification to prepare high-performance fibers, *Nano Mater. Sci.*, 2023, **5**(1), 1–14, DOI: [10.1016/j.nanoms.2021.11.004](https://doi.org/10.1016/j.nanoms.2021.11.004).
- 13 M. Xu, Y. Zhang and L. Zhang, Editorial for a special issue on: (photo)electrochemical materials and devices, *Nano Mater. Sci.*, 2023, **5**(2), 117–118, DOI: [10.1016/j.nanoms.2023.06.003](https://doi.org/10.1016/j.nanoms.2023.06.003).
- 14 J. Peng, *et al.*, Recent advances in 2D transition metal compounds for electrocatalytic full water splitting in



- neutral media, *Mater. Today Adv.*, 2020, **8**, 100081, DOI: [10.1016/j.mtadv.2020.100081](https://doi.org/10.1016/j.mtadv.2020.100081).
- 15 Q. Xiang and J. Yu, Graphene-Based Photocatalysts for Hydrogen Generation, *J. Phys. Chem. Lett.*, 2013, **4**(5), 753–759, DOI: [10.1021/jz302048d](https://doi.org/10.1021/jz302048d).
- 16 Z. Huang, *et al.*, Structures, properties and application of 2D mono-elemental materials (Xenes) as graphene analogues under defect engineering, *Nano Today*, 2020, **35**, 100906, DOI: [10.1016/j.nantod.2020.100906](https://doi.org/10.1016/j.nantod.2020.100906).
- 17 B. Shanmughan, A. Nighojkar and B. Kandasubramanian, Exploring the future of 2D catalysts for clean and sustainable hydrogen production, *Int. J. Hydrogen Energy*, 2023, **48**(74), 28679–28693, DOI: [10.1016/j.ijhydene.2023.04.053](https://doi.org/10.1016/j.ijhydene.2023.04.053).
- 18 K. Ledwaba, S. Karimzadeh and T.-C. Jen, Emerging borophene two-dimensional nanomaterials for hydrogen storage, *Materials Today Sustainability*, 2023, **22**, 100412, DOI: [10.1016/j.mtsust.2023.100412](https://doi.org/10.1016/j.mtsust.2023.100412).
- 19 H. Wang, *et al.*, Co-Ru alloy nanoparticles decorated onto two-dimensional nitrogen doped carbon nanosheets towards hydrogen/oxygen evolution reaction and oxygen reduction reaction, *J. Energy Chem.*, 2023, **87**, 286–294, DOI: [10.1016/j.jechem.2023.08.039](https://doi.org/10.1016/j.jechem.2023.08.039).
- 20 X. Jin, T.-H. Gu, K.-G. Lee, M. J. Kim, M. S. Islam and S.-J. Hwang, Unique advantages of 2D inorganic nanosheets in exploring high-performance electrocatalysts: synthesis, application, and perspective, *Coord. Chem. Rev.*, 2020, **415**, 213280, DOI: [10.1016/j.ccr.2020.213280](https://doi.org/10.1016/j.ccr.2020.213280).
- 21 Y. Wei, F. Gao, H. Huang and G. Jiang, Two-dimensional B<sub>7</sub>P<sub>2</sub>: Dual-purpose functional material for hydrogen evolution reaction/hydrogen storage, *Int. J. Hydrogen Energy*, 2022, **47**(13), 8338–8347, DOI: [10.1016/j.ijhydene.2021.12.210](https://doi.org/10.1016/j.ijhydene.2021.12.210).
- 22 L. Zhang, N. Wang and Y. Li, Design, synthesis, and application of some two-dimensional materials, *Chem. Sci.*, 2023, **14**(20), 5266–5290, DOI: [10.1039/D3SC00487B](https://doi.org/10.1039/D3SC00487B).
- 23 L. Tang, X. Meng, D. Deng and X. Bao, Confinement Catalysis with 2D Materials for Energy Conversion, *Adv. Mater.*, 2019, **31**(50), 1901996, DOI: [10.1002/adma.201901996](https://doi.org/10.1002/adma.201901996).
- 24 K. S. Kim, *et al.*, Continuous synthesis of high-entropy alloy nanoparticles by in-flight alloying of elemental metals, *Nat. Commun.*, 2024, **15**(1), 1450, DOI: [10.1038/s41467-024-45731-z](https://doi.org/10.1038/s41467-024-45731-z).
- 25 P. K. Sahoo, S. R. Bisoi, Y.-J. Huang, D.-S. Tsai and C.-P. Lee, 2D-Layered Non-Precious Electrocatalysts for Hydrogen Evolution Reaction: Fundamentals to Applications, *Catalysts*, 2021, **11**(6), 689, DOI: [10.3390/catal11060689](https://doi.org/10.3390/catal11060689).
- 26 Z. Wu, *et al.*, Microwave Phosphine-Plasma-Assisted Ultrafast Synthesis of Halogen-Doped Ru/RuP<sub>2</sub> with Surface Intermediate Adsorption Modulation for Efficient Alkaline Hydrogen Evolution Reaction, *Adv. Mater.*, 2024, **36**(13), 2311018, DOI: [10.1002/adma.202311018](https://doi.org/10.1002/adma.202311018).
- 27 W. K. Fan, A. Sherryana and M. Tahir, Advances in Titanium Carbide (Ti<sub>3</sub>C<sub>2</sub>T<sub>x</sub>) MXenes and Their Metal–Organic Framework (MOF)-Based Nanotextures for Solar Energy Applications: A Review, *ACS Omega*, 2022, **7**(43), 38158–38192, DOI: [10.1021/acsomega.2c05030](https://doi.org/10.1021/acsomega.2c05030).
- 28 R. M. Ronchi, J. T. Arantes and S. F. Santos, Synthesis, structure, properties and applications of MXenes: current status and perspectives, *Ceram. Int.*, 2019, **45**(15), 18167–18188, DOI: [10.1016/j.ceramint.2019.06.114](https://doi.org/10.1016/j.ceramint.2019.06.114).
- 29 K. R. G. Lim, M. Shekhirev, B. C. Wyatt, B. Anasori, Y. Gogotsi and Z. W. Seh, Fundamentals of MXene synthesis, *Nat. Synth.*, 2022, **1**(8), 601–614, DOI: [10.1038/s44160-022-00104-6](https://doi.org/10.1038/s44160-022-00104-6).
- 30 S. Venkateshalu, *et al.*, Recent advances in MXenes: beyond Ti-only systems, *J. Mater. Chem. A*, 2023, **11**(25), 13107–13132, DOI: [10.1039/D3TA01590D](https://doi.org/10.1039/D3TA01590D).
- 31 R. Mohili, N. R. Hemanth, K. Lee and N. K. Chaudhari, MXene-transition metal compound sulfide and phosphide hetero-nanostructures for photoelectrochemical water splitting, in *Solar-Driven Green Hydrogen Generation and Storage*, Elsevier, 2023, pp. 129–139, DOI: [10.1016/B978-0-323-99580-1.00008-X](https://doi.org/10.1016/B978-0-323-99580-1.00008-X).
- 32 S. Venkateshalu, *et al.*, Synergistic MXene/LDH heterostructures with extensive interfacing as emerging energy conversion and storage materials, *J. Mater. Chem. A*, 2023, **11**(27), 14469–14488, DOI: [10.1039/D3TA01992F](https://doi.org/10.1039/D3TA01992F).
- 33 J. Aravind, *et al.*, Chemosphere methods of synthesis, characteristics, and environmental applications of MXene: a comprehensive review, *Chemosphere*, 2022, **286**(P1), 131607, DOI: [10.1016/j.chemosphere.2021.131607](https://doi.org/10.1016/j.chemosphere.2021.131607).
- 34 Z. Wang, J. Xuan, Z. Zhao, Q. Li and F. Geng, Versatile Cutting Method for Producing Fluorescent Ultrasmall MXene Sheets, *ACS Nano*, 2017, **11**(11), 11559–11565, DOI: [10.1021/acsnano.7b06476](https://doi.org/10.1021/acsnano.7b06476).
- 35 S. Nam, S. Umrao, S. Oh, K. H. Shin, H. S. Park and I.-K. Oh, Sonochemical self-growth of functionalized titanium carbide nanorods on Ti<sub>3</sub>C<sub>2</sub> nanosheets for high capacity anode for lithium-ion batteries, *Composites, Part B*, 2020, **181**, 107583, DOI: [10.1016/j.compositesb.2019.107583](https://doi.org/10.1016/j.compositesb.2019.107583).
- 36 A. J. Y. Wong, K. R. G. Lim and Z. W. Seh, Fluoride-free synthesis and long-term stabilization of MXenes, *J. Mater. Res.*, 2022, **37**(22), 3988–3997, DOI: [10.1557/s43578-022-00680-5](https://doi.org/10.1557/s43578-022-00680-5).
- 37 Y. Feng, M. Zhang, H. Yan, Y. Zhang, R. Guo and H. Wang, Microwave-assisted efficient exfoliation of MXene and its composite for high-performance supercapacitors, *Ceram. Int.*, 2022, **48**(7), 9518–9526, DOI: [10.1016/j.ceramint.2021.12.149](https://doi.org/10.1016/j.ceramint.2021.12.149).
- 38 H. M. A. Hassan, *et al.*, Microwave synthesis of graphene sheets supporting metal nanocrystals in aqueous and organic media, *J. Mater. Chem.*, 2009, **19**(23), 3832, DOI: [10.1039/b906253j](https://doi.org/10.1039/b906253j).
- 39 T. Zhang, *et al.*, Synthesis of two-dimensional Ti<sub>3</sub>C<sub>2</sub>T<sub>x</sub> MXene using HCl+LiF etchant: enhanced exfoliation and delamination, *J. Alloys Compd.*, 2017, **695**, 818–826, DOI: [10.1016/j.jallcom.2016.10.127](https://doi.org/10.1016/j.jallcom.2016.10.127).
- 40 Y. Pei, *et al.*, Ti<sub>3</sub>C<sub>2</sub>T<sub>x</sub> MXene for Sensing Applications: Recent Progress, Design Principles, and Future Perspectives, *ACS Nano*, 2021, **15**(3), 3996–4017, DOI: [10.1021/acsnano.1c00248](https://doi.org/10.1021/acsnano.1c00248).



- 41 X. Sang, *et al.*, Atomic Defects in Monolayer Titanium Carbide ( $\text{Ti}_3\text{C}_2\text{T}_x$ ) MXene, *ACS Nano*, 2016, **10**(10), 9193–9200, DOI: [10.1021/acs.nano.6b05240](https://doi.org/10.1021/acs.nano.6b05240).
- 42 I. A. Poimenidis, *et al.*, Electrodeposited Ni foam electrodes for increased hydrogen production in alkaline electrolysis, *Fuel*, 2023, **342**, 127798, DOI: [10.1016/j.fuel.2023.127798](https://doi.org/10.1016/j.fuel.2023.127798).
- 43 K. Hou, Y. Yang, H. Zhou, X. Chen and S. Ge, Enhanced Yield of Large-Sized  $\text{Ti}_3\text{C}_2\text{T}_x$  MXene Polymers Nanosheets via Cyclic Ultrasonic-Centrifugal Separation, *Polymers*, 2023, **15**(6), 1330, DOI: [10.3390/polym15061330](https://doi.org/10.3390/polym15061330).
- 44 W. Feng, *et al.*,  $\text{Ti}_3\text{C}_2$  MXene: a promising microwave absorbing material, *RSC Adv.*, 2018, **8**(5), 2398–2403, DOI: [10.1039/C7RA12616F](https://doi.org/10.1039/C7RA12616F).
- 45 E. Satheeshkumar, T. Makaryan, A. Melikyan, H. Minassian, Y. Gogotsi and M. Yoshimura, One-step Solution Processing of Ag, Au and Pd@MXene Hybrids for SERS, *Sci. Rep.*, 2016, **6**(1), 32049, DOI: [10.1038/srep32049](https://doi.org/10.1038/srep32049).
- 46 M. Mahmood, *et al.*, Synthesis of Ultrathin  $\text{MnO}_2$  Nanowire-Intercalated 2D-MXenes for High-Performance Hybrid Supercapacitors, *Energy Fuels*, 2021, **35**(4), 3469–3478, DOI: [10.1021/acs.energyfuels.0c03939](https://doi.org/10.1021/acs.energyfuels.0c03939).
- 47 Y.-U. Haq, *et al.*, Synthesis and characterization of 2D MXene: device fabrication for humidity sensing, *J. Sci.: Adv. Mater. Devices*, 2022, **7**(1), 100390, DOI: [10.1016/j.jsamd.2021.08.003](https://doi.org/10.1016/j.jsamd.2021.08.003).
- 48 N. C. Osti, *et al.*, Effect of Metal Ion Intercalation on the Structure of MXene and Water Dynamics on Its Internal Surfaces, *ACS Appl. Mater. Interfaces*, 2016, **8**(14), 8859–8863, DOI: [10.1021/acsami.6b01490](https://doi.org/10.1021/acsami.6b01490).
- 49 W. Feng, *et al.*, Ni-modified  $\text{Ti}_3\text{C}_2$  MXene with enhanced microwave absorbing ability, *Mater. Chem. Front.*, 2018, **2**(12), 2320–2326, DOI: [10.1039/C8QM00436F](https://doi.org/10.1039/C8QM00436F).
- 50 S. You, T. Guo, P. Liu, X. Mao and Y. Zhang, Precipitation of monosodium aluminate hydrate from concentrated sodium aluminate solution, *Hydrometallurgy*, 2019, **183**, 125–129, DOI: [10.1016/j.hydromet.2018.12.005](https://doi.org/10.1016/j.hydromet.2018.12.005).
- 51 S. Kahraman, A. N. Canpolat and M. Fener, The influence of microwave treatment on the compressive and tensile strength of igneous rocks, *International Journal of Rock Mechanics and Mining Sciences*, 2020, **129**(2019), 104303, DOI: [10.1016/j.ijrmms.2020.104303](https://doi.org/10.1016/j.ijrmms.2020.104303).
- 52 M. Yu, Z. Wang, J. Liu, F. Sun, P. Yang and J. Qiu, A hierarchically porous and hydrophilic 3D nickel-iron/MXene electrode for accelerating oxygen and hydrogen evolution at high current densities, *Nano Energy*, 2019, **63**, 103880, DOI: [10.1016/j.nanoen.2019.103880](https://doi.org/10.1016/j.nanoen.2019.103880).
- 53 J. Wang, Y. Liu and G. Yang, Cobalt decorated ultra-thin  $\text{Ti}_3\text{C}_2$  MXene electrocatalyst for high-efficiency hydrogen evolution reaction, *Mater. Res. Express*, 2018, **6**(2), 025056, DOI: [10.1088/2053-1591/aaf1f0](https://doi.org/10.1088/2053-1591/aaf1f0).
- 54 Z. Shao, L. Wu, H. Ye, X. Ma, X. Zhang and L. Li, Promoting effect of MXenes on 1T/2H-MoSe<sub>2</sub> for hydrogen evolution, *CrystEngComm*, 2021, **23**(27), 4752–4759, DOI: [10.1039/D1CE00675D](https://doi.org/10.1039/D1CE00675D).
- 55 L. P. Hao, *et al.*, Synergistic Integration of MXene and Metal-Organic Frameworks for Enhanced Electrocatalytic Hydrogen Evolution in an Alkaline Environment, *Catalysts*, 2023, **13**(5), 802, DOI: [10.3390/catal13050802](https://doi.org/10.3390/catal13050802).
- 56 B. Wang, Q. Shu, H. Chen, X. Xing, Q. Wu and L. Zhang, Copper-Decorated  $\text{Ti}_3\text{C}_2\text{T}_x$  MXene Electrocatalyst for Hydrogen Evolution Reaction, *Metals*, 2022, **12**(12), 2022, DOI: [10.3390/met12122022](https://doi.org/10.3390/met12122022).
- 57 B. Unnikrishnan, *et al.*, Synthesis and in situ sulfidation of molybdenum carbide MXene using fluorine-free etchant for electrocatalytic hydrogen evolution reactions, *J. Colloid Interface Sci.*, 2022, **628**, 849–857, DOI: [10.1016/j.jcis.2022.07.176](https://doi.org/10.1016/j.jcis.2022.07.176).
- 58 S. Kumar, Fluorine-Free MXenes: Recent Advances, Synthesis Strategies, and Mechanisms, *Small*, 2023, **20**, 2308225, DOI: [10.1002/smll.202308225](https://doi.org/10.1002/smll.202308225).
- 59 Y. Jiang, *et al.*, Oxygen-Functionalized Ultrathin  $\text{Ti}_3\text{C}_2\text{T}_x$  MXene for Enhanced Electrocatalytic Hydrogen Evolution, *ChemSusChem*, 2019, **12**(7), 1368–1373, DOI: [10.1002/cssc.201803032](https://doi.org/10.1002/cssc.201803032).
- 60 B. Sarfraz, *et al.*, Bifunctional CuS/Cl-terminated greener MXene electrocatalyst for efficient hydrogen production by water splitting, *RSC Adv.*, 2023, **13**(32), 22017–22028, DOI: [10.1039/D3RA02581K](https://doi.org/10.1039/D3RA02581K).
- 61 N. H. Khadry and M. A. Ghanem, RSC advances highly dispersed platinum nanoparticles supported, *RSC Adv.*, 2014, **4**, 50114–50122, DOI: [10.1039/C4RA09341K](https://doi.org/10.1039/C4RA09341K).
- 62 S. A. Sergiienko, *et al.*, MXene-containing composite electrodes for hydrogen evolution: material design aspects and approaches for electrode fabrication, *Int. J. Hydrogen Energy*, 2021, **46**(21), 11636–11651, DOI: [10.1016/j.ijhydene.2021.01.041](https://doi.org/10.1016/j.ijhydene.2021.01.041).
- 63 I. Mubeen, S. Shah, E. Pervaiz and W. Miran, The promising frontier for next-generation energy storage and clean energy production: a review on synthesis and applications of MXenes, *Mater. Sci. Energy Technol.*, 2024, **7**, 180–194, DOI: [10.1016/j.mset.2023.10.002](https://doi.org/10.1016/j.mset.2023.10.002).
- 64 Z. Ai, *et al.*, Interface engineering in the BNNS@ $\text{Ti}_3\text{C}_2$  intercalation structure for enhanced electrocatalytic hydrogen evolution, *New J. Chem.*, 2019, **43**(22), 8613–8619, DOI: [10.1039/C9NJ01504C](https://doi.org/10.1039/C9NJ01504C).
- 65 B. Li, R. Ye, Q. Wang, X. Liu, P. Fang and J. Hu, Facile synthesis of coral-like Pt nanoparticles/MXene ( $\text{Ti}_3\text{C}_2\text{T}_x$ ) with efficient hydrogen evolution reaction activity, *Ionics*, 2021, **27**(3), 1221–1231, DOI: [10.1007/s11581-020-03884-z](https://doi.org/10.1007/s11581-020-03884-z).

